International Conference on Space Optics—ICSO 2022

Dubrovnik, Croatia

3–7 October 2022

Edited by Kyriaki Minoglou, Nikos Karafolas, and Bruno Cugny,

LEXI Segmented Slumped Micropore Optic Calibration at PANTER

LEXI Segmented Slumped Micropore Optic Calibration at PANTER

K. D. Kuntz[a], Vadim Burwitz[b], Rousseau Nutter[c], Cadin Connor[d], Gisela Hartner[b], Thomas Müller[b], Catriana Paw U[d], F. Scott Porter[e], Surangkhana Rukdee[b], Thomas Schmidt[b], and Brian Walsh[d]

[a]Johns Hopkins University, 3400 North Charles Street, Baltimore, MD, USA
[b]MPI für extraterrestrische Physik, Giessenbachstrasse, 85748 Garching, Germany
[c]Howard University/NASA GSFC, Greenbelt, MD, USA
[d]Boston University, 110 Cummington Mall, Boston, MA, USA
[e]NASA GSFC, Greenbelt, MD, USA

ABSTRACT

LEXI is a wide-field X-ray imager using bare-glass slumped micropore optics. The LEXI optic was recently characterized at PANTER to measure both the point spread function and the effective area as a function of energy. The effective area measurements were made with a continuum source in order to characterize the effective area curve at moderate energy resolution over the 0.2-4.0 keV range. Comparison of measurements with ray-tracing suggests a number of ways modeling can be improved in the future.

Keywords: X-ray optics, micropore optics, lobster-eye optics, PANTER, calibration,

1. INTRODUCTION

The Lunar Environment heliospheric X-ray Imager (LEXI[1]) is a small self-contained X-ray telescope intended to operate on the lunar surface to observe solar wind charge exchange (SWCX) emission originating in the Earth's magnetosheath due to the interaction of high-state ions in the compressed solar wind with the outer reaches of the Earth's exosphere. The SWCX emission in the magnetosheath is of great interest to heliosphericists, as it allows, for the first time, direct imaging of the structure of the magnetic field within the magnetosphere, and will allow one to directly track the effects of reconnection by measuring the extent to which the magnetopause moves when signatures of reconnection are seen elsewhere. The SWCX emission in the magnetosheath is of interest to astrophysicists because it is a highly time variable foreground in the same emission lines generally used for plasma diagnostics; unless the SWCX can be characterized, minimized, or removed, it poses a significant problem in understanding X-ray emission from the Galaxy and beyond.

In order to image a substantial portion of the nose of the Earth's magnetosheath, LEXI is a wide field ($\sim9°$ by $\sim9°$) soft (~0.1 to ~2.0 keV) X-ray telescope utilizing "lobster-eye" optics, also known as slumped micropore optics (SMPO). SMPO use square-pore glass microchannel plates to focus X-rays at grazing incidence in two dimensions. The optics are very lightweight while still robust, surviving harsh sounding rocket launches. The optics have short focal lengths and provide a rather unusual cruciform point spread function (PSF) with a strong central core of $10'$ to $15'$, an example of which is shown in Figure 1. Note that because the focussing planes are perpendicular to one another, the optic has inherent Cartesian axes. Although each individual microchannel plate or *facet* is small, they can be mosaicked to produce very large fields of view with an angular resolution that is small compared to the size of the FOV.

The LEXI optic (Figure 1) is a three by three mosaic of 40 mm by 40 mm facets manufactured by Photonis. Each facet was specified to have a radius of curvature (R_C) of 750 mm and is set into an aluminum frame machined to hold the facets on the surface of a sphere with R_C=750 mm. Each facet directly supports an optical

---

Further author information: (Send correspondence to K.D.K.)
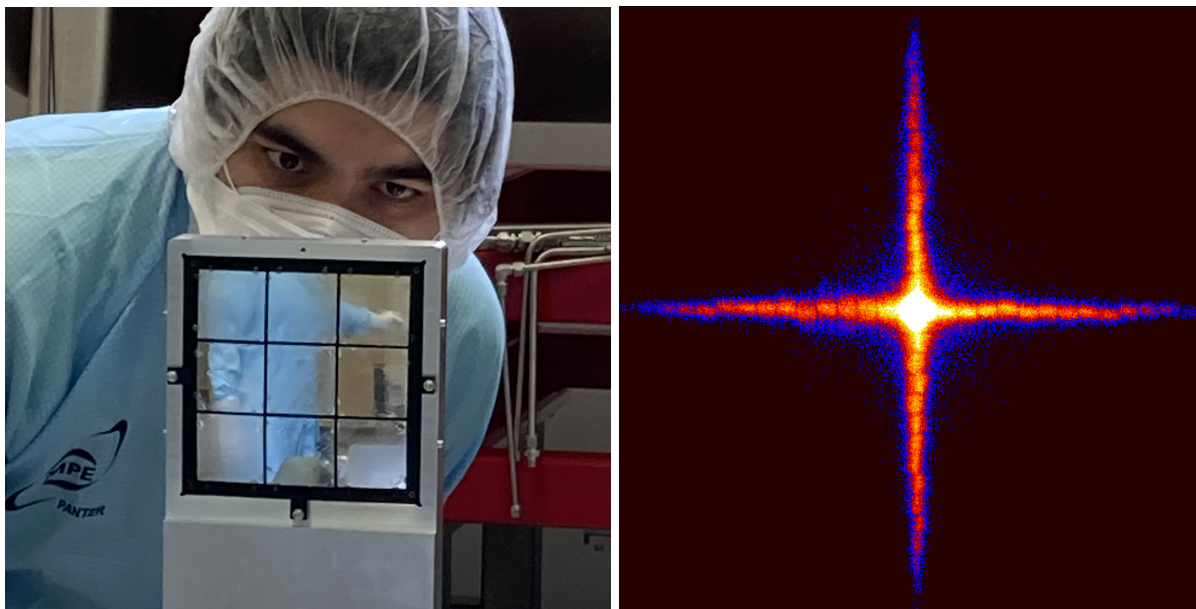K.D.K.: E-mail: kkuntz1@jhu.edu, Telephone: 1 410 512 5829

Figure 1. *Left:* The LEXI optic in its holder. *Right:* The PSF for the central facet of LEXI taken with the PIXI camera at PANTER. The image is $\sim 4.1°$ across and has been stretched to show the details of the arms of the PSF. The periodic dark lines roughly every $13'$ are due to sub-bundles of pores in the SMPO.

blocking filter (OBF) that is formed of a 200 nm film of LUXFilm® Polyimide and 30 nm of Al, which were applied by the Luxel Corporation. Most SMPO used in astrophysics are coated with iridium to increase their reflectivity. However, the LEXI SMPOs are bare glass, due to time and other constraints, which poses some unique calibration challenges.

The baseline calibration program for LEXI, so that its data can be used in a fully quantitative way, requires both knowledge of the effective area (or throughput) of the optic and knowledge of the size of the PSF, both as a function of the angle of incidence and as a function of energy. Unlike many types of optics, only a small portion of the optic contributes to focussing X-rays from a given direction. Thus, calibration of the LEXI optic, in essence, requires the characterization of each facet, individually. The SWCX emission that is the object of the LEXI study, as well as the bulk of the X-ray background to that emission, is primarily below 1-2 keV, while the OBF effectively cuts off the emission below 0.1 keV. Thus, the effective area and the PSF needed to be characterized over the 0.1-2.0 keV energy range.

2. METHOD AND RESULTS

The LEXI optic calibration was done at the PANTER facility[2,3] in Neuried in the southwest of Munich over 21-25 February and 20-29 April 2022. PANTER is a facility of the Max-Planck-Institut für extraterrestrische Physik in Garching. The PANTER vacuum beamline is 120 m long, with a further 12 m long chamber, so that beam divergence is minimized. Two different CCD detectors can be used to characterize the optic (see Table 1) while an Amptek silicon drift detector (SDD) can be used to monitor the beam stability. The beam itself is provided by a very well characterized electron impact source with one of a number of targets.

2.1 Focus and PSF

The initial specification of the individual facets was R_C=750 mm. At Goddard Space Flight Center we used a ~ 1 m long test chamber to measure the radius of curvature of each facet. With an X-ray source near the focus of the facet, a mask, and a CCD detector on the opposite side of the facet, one can determine the radius of curvature accurately. The facets chosen for the flight optic had a mean R_C=725 mm with a variation of σ_{R_C}=11.3 mm. However, the frame that holds the individual facets had already been machined to R_C=750 mm.

Table 1. PANTER Instruments.

Instrument	Size (pixels)	Pixel Size	Scale	Area
PIXI	1340×1300	20 μm	0.189 arcmin/pixel	6.968 cm^2
TRoPIC	256×256	75 μm	0.708 arcmin/pixel	3.516 cm^2*
SDD	1			0.25 cm^2

*Only the central 250×250 pixels are used.

Since the focal length is half the radius of curvature, the difference in focal length between the facets and the frame is ~12.5 mm. This facet/frame mismatch means that a source lying in the direction of the intersection of facets will be focussed in a slightly different location by each of the facets contributing to the focus.

Due to its smaller pixel size and larger format, PIXI was used to make the focus search. Due to its strength, the detector response, and the assumed optic throughput, we used the Al-K (1.49 keV) line source. A focus search for the central facet, when the beam was masked to fall only on the central facet found a focal length of 364 mm, which is precisely what was expected from the R_C measurements in the GSFC test chamber. To determine the extent of the facet/frame mismatch, we aligned the beam to each intersection of four facets (the corners of the central facet) and, without masking the beam, determined the distance to the detector that minimized the angular distances between the four separate image spots. Although there was quite a bit of variation among the four four-facet intersections, the distance that minimized the image spot was roughly the focal length of the frame, 375 mm.

In order to produce the most uniform image across the FOV, it was decided to characterize the optics at the design focus, 375 mm. However, the PSF size was also measured for each facet at the mean radius of curvature. Those results are listed in Table 2. Note that since each facet can have a different curvature in one direction than it does in the other, both dimensions are listed.

Table 2. FWHM of the PSF at the detector of each facet.

Facet	Best Focus		Design Focus	
	X	Y	X	Y
Upper Left	11.36′	12.37′	15.72′	17.28′
Upper Center	11.89′	11.77′	17.35′	16.52′
Upper Right	10.92′	10.31′	13.60′	14.46 ′
Center Left	10.44′	12.92′	15.43′	19.53′
Center	9.52′	9.26′	12.43′	12.92′
Center Right	11.62′	10.23′	10.74′	10.57′
Bottom Left	14.91′	13.95′	20.42′	19.89′
Bottom Center	10.50′	10.10′	12.76′	13.62′
Bottom Right	14.60′	12.64′	11.31′	12.07′

2.2 Effective Area

It has been traditional, particularly with detectors with very limited energy resolution, to use strong X-ray lines to characterize the effective area at a limited number of discrete energies. Although this procedure allows one to then reconstruct the effective area for a particular input spectral shape, it is liable to errors near instrumental edges, where the reflectivity changes rapidly over a small energy range. However, given detectors with good energy resolution, one can characterize the effective area over the entire energy range of interest using an X-ray
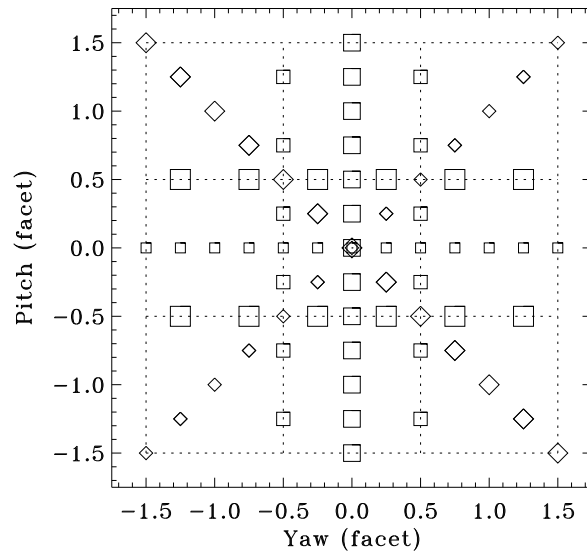
Figure 2. Pattern of the directions at which the effective areas were measured. The dotted lines indicate facet boundaries. The closest spacing of locations is 0.79°, which is a quarter of a facet.

continuum source; the resolution around edges becomes a matter of the line spread function of the detector and the accumulated number of counts at that energy.

To characterize the LEXI optic over the 0.1-2.0 keV range we used an aluminum target to produce a "very low energy" continuum in the 0.2-2.0 keV range that also includes the O-K line at 0.525 keV. In addition, we used a Ti target behind a 1 μm thick Ti filter to produce a "low energy" continuum in the 0.6-4.0 keV range. We also made traditional line-based measurements in a variety of lines (see Table 3) to confirm the continuum measurements and to provide higher signal to noise images for PSF characterization.

Table 3. FWHM of the PSF of each facet.

Line	Energy	Time/Position	Positions
B-K	0.183 keV	600 s	25
C-K	0.277 keV	300 s	13
Ti-L*	0.452 keV	600 s	13
O-K*	0.525 keV	600 s	76
Cu-L	0.929 keV	180 s	25
Al-K	1.49 keV	180 s	26
Ag-L	2.98 keV	180 s	13

* Lines embedded in the continuum exposures.

We used the TRoPIC detector to measure the effective area with the very low energy continuum in 73 positions, spaced roughly 0.76° (or a quarter of a facet) apart (see Figure 2 and Figure 3) with a higher density of measurements in the center of the FOV. Further measurements were made with the low energy continuum and lines, primarily in the central column of facets, where the nose of the magnetopause will be placed. For each series of measurements, "flat field" images were taken when the optic was not between the source and the detector, the optic was then moved into position for the series of measurements, and then flat fields were taken after the series. The flat field images were used to determine the effective area, while the SDD measurements
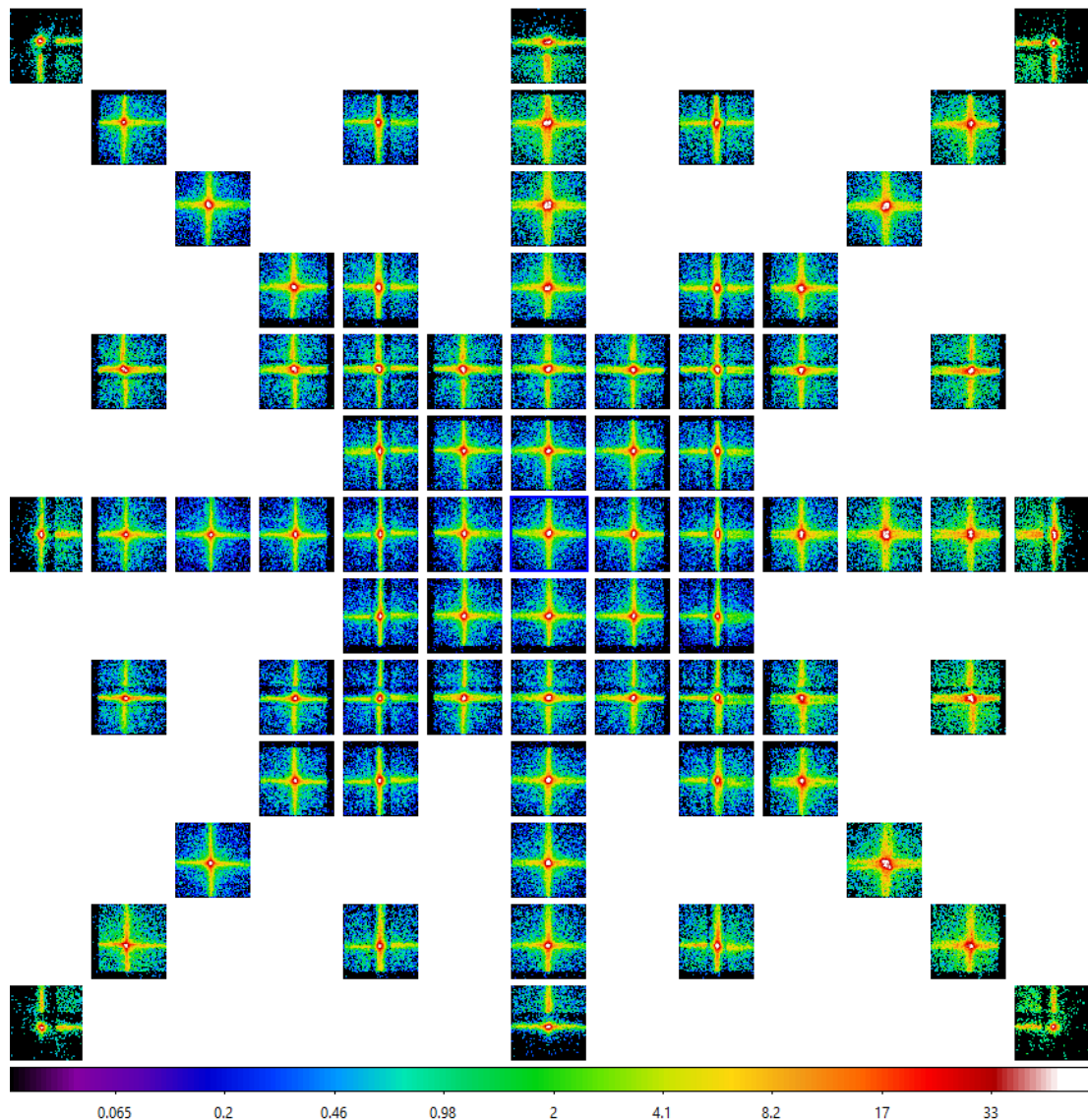
Figure 3. Images of the PSF at O-K (0.525 keV) obtained from the very low energy continuum measurements. Comparison with the Figure 2 will show which images were taken with the source in the direction of the frame.

taken during the series were used to correct for small timescale variations in the beam, under the assumption that the beam behaves synchronously for all energies.

Figure 4 shows the effective area curve for the center of the center facet. (This is essentially the spectrum taken through the optic divided by the flat field spectrum, multiplied by the area of the detector and a geometric correction factor.) The results of the line measurements have been over-plotted. Uncertainties in the continuum measurements are ~1.5(~6)% at 0.5(1.0) keV and ~5(~7)% at 2.0(3.0) keV. It is clear that the effective area as a function of energy is very well characterized, even if the model seems to be significantly awry.

3. COMPARISON TO THEORY

Our model for the effective area of the optic was derived from a Pore-By-Pore (PBP) ray-tracing routine* using reflectivities for SiO_2 from henke.lbl.gov. This effective area was then multiplied by the transmission of the OBF,

---
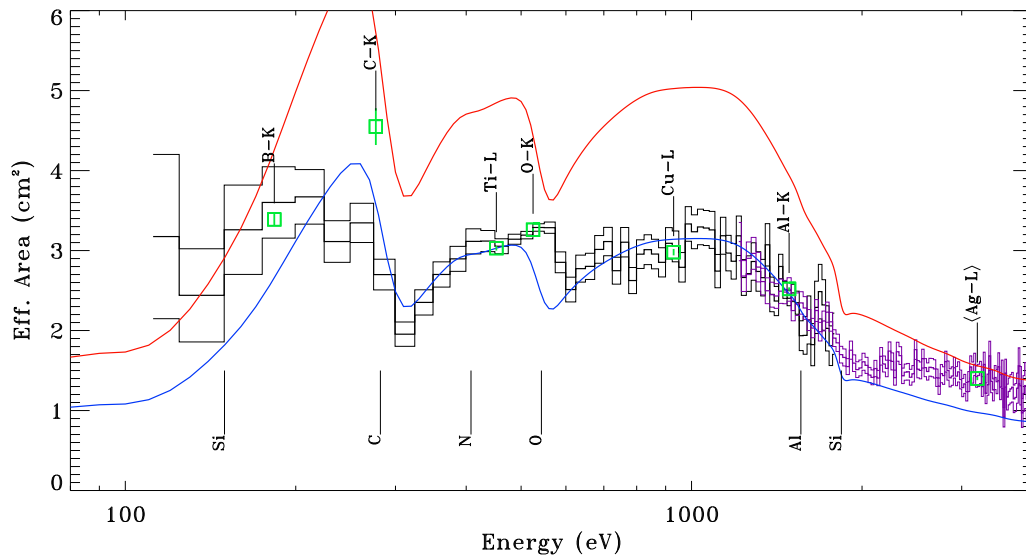
*See pages.jh.edu/kkuntz1/ for further documentation.

Figure 4. The effective area as a function of energy for the center of the center facet. The thick black line is the data from the very low energy continuum; the thin black lines show the uncertainty. The purple line is the data from the low energy continuum; the uncertainty is also shown. The red line is a theoretical model of this optic. The blue line is the model reduced by a factor of 1.6. The green boxes with error bars show effective areas derived from the individual line measurements. The notation below the data indicates the various absorption edges in the absence of smoothing.

and convolved with an approximate spectral line spread function (LSF) of the TRoPIC detector. The effective area function of the optic is expected to show absorption edges at 0.099, 0.149, and 1.839 keV from the Si, and 0.543 from the O. The OBF introduces edges at $\sim$0.072 and 1.559 keV (Al), 0.284 keV (C), 0.408 keV (N), and increases the depth of the O edge at 0.543 keV. The binning of the data and the smearing by the LSF cause the absorption edges to be not quite so sharp as one would expect, and obscures the relatively shallow edges due to N and Al.

Scaling the model by a constant factor does not produce the observed function; when the region between the O edge and the Si edge is well fit, the higher energy region is not, suggesting that the scaling is a function of energy. We also note that the area around the O edge is not well fit. There is some uncertainty in the amount of O in the OBF due to the oxidation of the Al, however that uncertainty is much smaller than the discrepancy here. The area below $E{\sim}0.2$ keV is not well fit either, however the beam emission here is rather weak and there are significant systematic uncertainties.

The discrepancy between measurement and model is not, to first order, surprising. There are a number of uncertainties concerning the reflectivities. First, the composition of the glass is proprietary, so it is not known to the experimenters. We have assumed that the reflectivity will be similar to that of SiO_2, and that trace ingredients will produce small edges. Second, we do not yet have measurements of the surface roughness within the SMPO pores. Previous work with Ir coated optics[4] showed that the optics had 85% to 95% the expected throughput, so our initial model assumed no surface roughness.

We can explore this problem more fully if we co-add the appropriate data. Figure 5 shows the vignetting function for each of the scans passing through the center of the center facet. Although different facets do show different effective areas, the centers of each facet are comparable because the bulk of the throughput for a given direction is due to a region on the optic that is roughly the size of a facet. We can thus average the data from analogous positions, in this case the center of each facet, to produce a higher signal to noise effective area curve, though its absolute value will need to be adjusted for any particular facet. This curve is shown in Figure 6. We do not see any further edges.
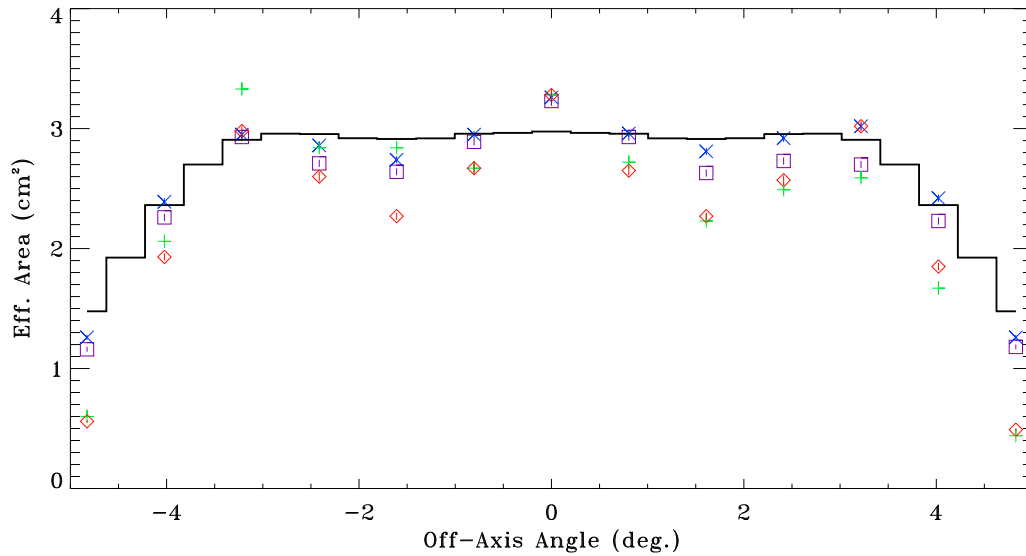
Figure 5. The effective area as a function of off-axis angle at 0.525 keV. Purple boxes: in the yaw direction, blue "x"s: in the pitch direction, green crosses: one diagonal, red diamonds: the other diagonal. The solid black line is a model vignetting function at the same energy, scaled to match the measurements.

We again see that the model does not fit the data but, with the exception of higher than expected effective areas at E<0.2 keV, the shape seems reasonable; the problem is mostly the amplitude of the curve. We can again extract reflectivities from henke.lbl.gov, but this time applying a surface roughness correction using the Nevot-Croce approximation. We extracted reflectivities for RMS surface roughnesses of 5, 6, 7, 8, 9, and 10 nm. As surface roughness increases, reflectivity decreases more rapidly at higher energies than lower energies, and reflectivity decreases more rapidly at more normal incidence angles than more grazing angles. Since the total throughput of an SMPO is a complex convolution of reflectivity and distance from the optical axis, it is not always clear what will happen.

What we see is a relatively modest decrease at the highest energies due to very few of the high energy photons being reflected and most of the throughput being due to collimation. We see strong decreases in the middle energies (0.5-2.0 keV), and not so strong decreases at the lowest energies. No single surface roughness provides a satisfactory fit, particularly around the O edge. Indeed, the shape of the effective area curve after correction for surface roughness is arguably worse than the scaled model for a perfectly smooth optic, particularly between the C and O edges. A 10 nm RMS roughness is an order of magnitude greater than expected, and yet that curve just barely fits the two sides of the Si edge, which suggests that surface roughness does not explain the bulk of the mismatch between the model and measurements.

There are a number of possible sources for the discrepancy; an inadequate formulation for the surface roughness correction, an inadequate formulation of the glass composition, or an inadequate spectral line spread function. We are actively pursuing alternate formulations for the application of surface roughness. A brief survey of different types of glass suggests that the largest differences in reflectivity occur above 1 keV, perhaps causing the discrepancy across the Si edge, but not at lower energies. While an inadequate LSF might explain part of the discrepancy at the O edge, given that the modeled location of the C and Si edges is good suggests that it is not the problem.

4. SUMMARY

Calibration of the LEXI optic at PANTER has exposed weaknesses in our capability to model SMPO with ray tracing while also indicating which improvements remain to be made in that modeling. Our PANTER results
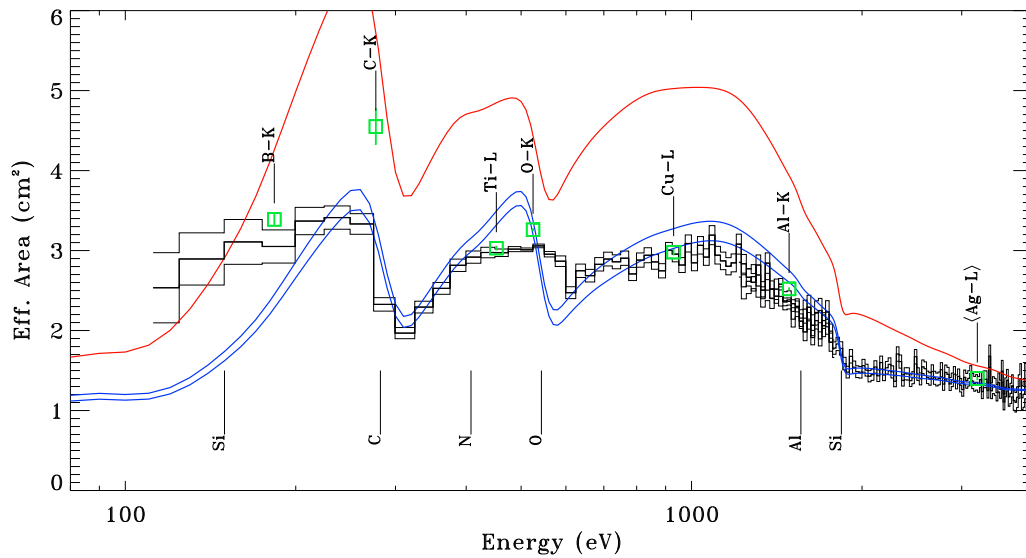
Figure 6. The effective area as a function of energy for the center of the facets. The very low energy continuum data are the average of eight measurements, while the low energy continuum data are the average of three measurements. The red line is the model of the effective area assuming no surface roughness. The blue lines are models with RMS surface roughnesses of 9 nm and 10 nm.

demonstrate that the LEXI optics will achieve a PSF smaller than $15'$ over most of its FOV, and we have characterized the PSF shape over the bulk of the FOV. The effective area curve is well characterized, even if the shape is not entirely understood.

ACKNOWLEDGMENTS

REFERENCES

[1] Walsh, B., Collier, M., Kuntz, K., Porter, F., Sibeck, D., Busk, S., Connor, H., Galeazzi, M., Naldoza, V., Sembay, S., Thomas, N., and Nutter, R., "Heliospheric imaging and science from the Moon with LEXI," in [*AGU Fall Meeting Abstracts*], **2021**, SH23A–06 (Dec. 2021).

[2] Bradshaw, M., Burwitz, V., Hartner, G., Pelliciari, C., Langmeier, A., Liao, Y., Friedrich, P., Valsecchi, G., Barrière, N., Collon, M. J., and Vacanti, G., "Developments in testing x-ray optics at MPE's PANTER facility," in [*Optics for EUV, X-Ray, and Gamma-Ray Astronomy IX*], *Society of Photo-Optical Instrumentation Engineers (SPIE) Conference Series* **11119**, 1111916 (Sept. 2019).

[3] Freyberg, M. J., Budau, B., Burkert, W., Friedrich, P., Hartner, G., Misaki, K., and Mühlegger, M., "New technology and techniques for x-ray mirror calibration at PANTER," in [*Space Telescopes and Instrumentation 2008: Ultraviolet to Gamma Ray*], Turner, M. J. L. and Flanagan, K. A., eds., *Society of Photo-Optical Instrumentation Engineers (SPIE) Conference Series* **7011**, 701117 (July 2008).

[4] Thomas, N. E., "Characterization of Slumped Micropore Optics," in [*AAS/High Energy Astrophysics Division*], *AAS/High Energy Astrophysics Division* **17**, 109.73 (Mar. 2019).